Published in final edited form as:
Neuroscience. 2010 December 15; 171(3): 924–933. doi:10.1016/j.neuroscience.2010.09.054.

Synaptic changes underlying the strengthening of GABA/glycinergic connections in the developing lateral superior olive

Gunsoo Kim[1] and **Karl Kandler**
Department of Otolaryngology, University of Pittsburgh School of Medicine, Biomedical Science Tower 3, 3501 Fifth Avenue, Pittsburgh, PA 15261

Abstract

Before hearing onset, the topographic organization of the auditory GABA/glycinergic pathway from the medial nucleus of the trapezoid body (MNTB) to the lateral superior olive (LSO) is refined by synaptic silencing and strengthening. The synaptic mechanisms underlying the developmental strengthening of maintained MNTB-LSO connections are unknown. Here we address this question using whole-cell recordings from LSO neurons in slices prepared from prehearing mice. Minimal and maximal stimulation techniques demonstrated that during the first two postnatal weeks, individual LSO neurons lose about 55% of their initial presynaptic MNTB partners while maintained single-fiber connections become about 14-fold stronger. Analysis of MNTB-evoked miniature events indicates that this strengthening is accompanied by a 2-fold increase in quantal amplitude. Strengthening is not caused by an increase in the probability of release because paired pulse ratios increased from 0.7 in newborn animals to 0.9 around hearing onset, indicating a developmental decrease rather than increase in release probability. In addition, a possible soma-dendritic relocation of MNTB input seems unlikely to underlie their strengthening as indicated by analysis of the rise times of synaptic currents argues. Taken together, we conclude that the developmental strengthening of MNTB-LSO connections is achieved by a 2-fold increase in quantal size and an 8-fold increase in quantal content.

Keywords

auditory; inhibitory; sound localization; refinement

Interaural sound level differences are a major cue by which mammals determine the direction of incoming sound. In the central nervous system interaural sound level differences are processed for the first time by binaural neurons in the lateral superior olive (LSO). LSO neurons receive excitatory inputs from the ipsilateral ear via a glutamatergic projection from the ipsilateral cochlear nucleus (CN) and receive inhibitory inputs from the contralateral ear via a glycinergic projection from the medial nucleus of the trapezoid body (MNTB) (Boudreau and Tsuchitani, 1968; Cant and Casseday, 1986; Sanes and Rubel, 1988; Bledsoe et al., 1990; Sommer et al., 1993). Both projections are tonotopically organized and aligned

Corresponding author. Karl Kandler, Department of Otolaryngology, University of Pittsburgh School of Medicine, Biomedical Science Tower 3, 3501 Fifth Avenue, Rm 10016, Pittsburgh, PA 15261, kkarl@pitt.edu, Phone: 412-624-8398, Fax: 412 383 5298.
[1]present address: Gunsoo Kim, PhD, Department of Physiology and Keck Center for Integrative Neuroscience, University of California San Francisco, San Francisco, CA 94143-0444

such that binaural LSO neurons receive excitatory and inhibitory inputs that are tuned to the same sound frequency (for review see (Tollin, 2003).

The precise tonotopic organization and physiological properties of the inhibitory MNTB-LSO pathway emerge gradually during development. The initial formation of the MNTB-LSO pathway takes place prenatally (Sanes and Siverls, 1991; Kandler and Friauf, 1993; Kandler and Friauf, 1995b) and is followed by a series of anatomical and physiological changes that occur both in presynaptic MNTB neurons and postsynaptic LSO neurons (Sanes and Friauf, 2000; Friauf, 2004; Kandler and Gillespie, 2005; Kandler et al., 2009). The majority of these changes occurs before animals can hear airborne sound and thus occur independently of auditory experience. In rats and mice, topographic refinement of the MNTB-LSO pathway before hearing onset (the first two postnatal weeks (Geal-Dor et al., 1993) is characterized by a silencing of most connections and a strengthening of maintained ones (Kim and Kandler, 2003; Noh et al., 2010). The magnitude of this pre-hearing reorganization is quite remarkable because single LSO neurons lose approximately 75% of their initial presynaptic MNTB partners while maintained connections become about 12-fold stronger. While these changes before hearing onset are crucial for the ability of LSO neurons to encode interaural intensity differences right at hearing onset (Sanes and Rubel, 1988), the mechanisms that underlie the pre-hearing strengthening of MNTB-LSO connections are unknown.

Work conducted in other brain areas indicated that the major mechanisms to increase the amplitude of GABAergic or glycinergic postsynaptic currents (PSCs) elicited by a single axon include an increase in quantal amplitude (Singer and Berger, 1999; Awatramani et al., 2005), in number of release sites (Juttner et al., 2001; Morales et al., 2002), or in presynaptic release probability (Kobayashi et al., 2008). To investigate whether and to what degree these pre- and postsynaptic mechanisms contribute to the strengthening of individual connections in the MNTB-LSO pathway, we compared the properties of MNTB-evoked synaptic responses in LSO neurons in slices prepared from newborn mice and mice around hearing onset. Our results demonstrate that the degree of refinement of the MNTB-LSO pathway in mice is highly similar to rats and further indicate that the strengthening of the maintained MNTB inputs is achieved by an approximate 2-fold increase in quantal amplitude and an over 8-fold increase in the quantal content of individual MNTB inputs.

Experimental procedure

Animals, slice preparation, and electrophysiology

Experimental procedures were in accordance with NIH guidelines and were approved by the IACUC at the University of Pittsburgh. All experiments were performed in brainstem slices prepared from mouse pups of the strain 129S6/SvEv aged between postnatal day (P) 1 and P 12. Although the 129S6/SvEv strain has a deletion variant of the Disc1 gene which causes slight abnormalities in working memory and other behavioral tests (Koike et al., 2006; Ishizuka et al., 2007), Disc 1 is not expressed in auditory brainstem neurons (Schurov et al., 2004) and its mutation therefore unlikely to influence early development of LSO circuitry.

Brainstem slices were prepared as described previously (Kim and Kandler, 2003; Kullmann and Kandler, 2008). Briefly, animals were anesthetized by hypothermia (P1-P3) or isoflurane (P10-12) before decapitation. Coronal slices (300 μm) were cut on a vibrating microtome (DTK-1500E, Ted Pella, Redding, CA, USA). Slices containing both the LSO and the MNTB were selected and allowed to recover in an interface-type chamber under 95%O_2/5%CO_2 atmosphere for 1~2 hours at RT (23°C). For slice preparation and incubation, 1 mM kynurenic acid was present in the ACSF (composition in mM: NaCl 124, $NaHCO_3$ 26, Glucose 10, KCl 5, KH_2PO_4 1.25, $MgSO_4$ 1.3, $CaCl_2$ 2, pH = 7.4 when

bubbled with 95%O_2/5%CO_2). For recordings, slices were transferred to a submerged-type chamber mounted to an upright microscope (BX50, Olympus) and superfused with oxygenated ACSF at RT at a rate of ~3-4 ml/min.

Electrophysiological recordings

Whole-cell voltage clamp recordings were obtained at RT from visually identified LSO principal neurons in the medial half of the LSO using an Axopatch 1D amplifier. Recording electrodes (2-3 MΩ) contained (in mM): 76 Cs-methanesulfonate, 56 CsCl, 10 EGTA, 1 $MgCl_2$, 1 $CaCl_2$, 2 ATP-Mg, 0.3 GTP-Na, 5 Na_2-phosphocreatine, and 10 HEPES (pH = 7.3, 290 mOsm). With the internal and external solution, E_{Cl} was -20 mV and LSO neurons were held at -70 mV (corrected for -5 mV liquid junction potential), resulting in -50 mV driving force for Cl^-. Patch electrodes with larger tip diameters (~ 1 MΩ) were used for electrical stimulation at the lateral edge of the MNTB. Constant current pulses (0.2 ms) were delivered using a stimulation isolation unit (IsoFlex, AMPI). All evoked PSCs including paired pulse responses were elicited at 0.2 Hz. Data were filtered at 2 kHz (Axopatch 1D) and acquired at 10 kHz using custom-written Labview data acquisition software (Kullmann and Kandler, 2001).

Minimal stimulation

Minimal stimulation techniques were used to record responses elicited by single MNTB axons (Stevens and Wang, 1994; Kim and Kandler, 2003). A stimulus-response relation was obtained and the first plateau was determined at which the failure rate decreased without increasing the mean amplitude of successful responses (see Figure 3B and D). Responses during this plateau were regarded as inputs by single-fibers, and 20-100 responses were evoked at 0.2 Hz. Only responses with latencies that fell into a 1 ms long window were accepted.

Evoked miniature PSC

To examine miniature PSCs (mPSCs) that are generated by MNTB terminals, MNTB fibers were stimulated in ACSF in which Ca^{2+} was replaced by equimolar Sr^{2+}. Under this condition, asynchronous release is promoted, and asynchronous events represent quantal events (Goda and Stevens, 1994; Behrends and ten Bruggencate, 1998). In 2 mM Sr^{2+} / 0 mM Ca^{2+}, PSCs evoked by electrical stimulation were markedly smaller than in normal 2 mM Ca^{2+} ACSF, and asynchronous events were observed. However, because in the LSO, single stimuli in Sr^{2+} ACSF rarely elicited asynchronous events we applied stimulus trains (2-10 pulses at 100 Hz). These train stimuli effectively induced asynchronous events at all ages examined. A one-second long base line was recorded prior to the stimulus train and another 1 second long trace was recorded after the train. To prevent contamination by spontaneous events, cells that showed high spontaneous activity during the baseline period were excluded from analysis.

Data analysis

Synaptic responses were analyzed using custom written Labview and MATLAB programs. Evoked mPSCs were identified and collected from a 3-400 ms window after the stimulus train using a sliding template method (Clements and Bekkers, 1997) implemented in MATLAB. The detection thresholds were set low, and false positives (events that did not exhibit a rapid rise followed by a typical decay time) were rejected by visual inspection. In P1-3 animals, asynchronous events often appeared only during the decay phase of the stimulus-locked responses. For these events, peak amplitude was measured after the baseline was adjusted by fitting a straight line to the baseline immediately before the peak (Lu and Trussell, 2000). Paired pulse ratios were computed from paired PSCs evoked by two stimuli

with intervals of 10, 20, 50, 100, 200, and 500 ms. At least 20 trials were averaged and then the mean second PSC peak amplitude was divided by the first (Kim and Alger, 2001). At short inter-pulse intervals (10, 20, and 50 ms in P1-3; 10 and 20 ms in P10-12), there was a significant overlap between the first and the second PSCs (Figure 5A). To accurately measure the peak amplitude of the second PSCs, a mean PSC from a longer interval was scaled and subtracted from the paired-pulse responses, isolating the second PSC. The coefficient of variation (CV) for peak amplitudes of paired PSCs was computed from 15-30 individual trials in each cell (Figure 5C). Throughout the text and figures, errors are expressed as standard error.

Results

Developmental changes in single-fiber and maximal MNTB inputs

Synaptic currents evoked by electrical stimulation of MNTB fibers were recorded from visually identified, uni- or bipolar mouse LSO neurons using whole-cell voltage clamp technique. Because recording electrodes contained a high Cl^- concentration (E_{Cl}: -20 mV), MNTB-elicited postsynaptic currents (PSCs) were inwardly directed. To isolate PSCs mediated by GABA and glycine receptors, all recordings were performed in the presence of the ionotropic glutamate receptor antagonist Kynurenic acid (1 mM). MNTB-evoked PSCs in P1-3 animals were small and had a slow time course (Figure 1A). As previously reported for rats and gerbils (Kotak et al., 1998; Nabekura et al., 2004), MNTB-evoked PSCs in the LSO of neonatal mice contained both bicuculline sensitive (10 μM) and strychnine sensitive (1 μM) components, indicating mixed release of GABA and glycine (Figure 1A, P1-2, n = 7). Around hearing onset, PSCs were larger and faster and were blocked by 1 μM strychnine (Figure 1A, P10-11, n = 5). Current-voltage relationships of MNTB-evoked PSCs were linear between -90 to + 40 mV (r = 0.998) with a reversal potential of -19.5 mV (P1-3) and -17.6 mV (P10-12, n = 3), close to the theoretical value determined by the Nernst Equation (E_{Cl} = -20 mV), indicating a good control of membrane voltage (Figure 1B).

We next investigated how the maximal MNTB inputs onto a single LSO neuron changes during the period before hearing onset in 129S6/SvEv mice. In both P1-3 as well as P10-12 animals, peak amplitudes of MNTB-evoked PSCs increased with increasing stimulus intensity, typically peaking between 200 to 400 μA and slightly decreasing at high stimulus intensities (>500 μA) possibly due to the damage of fibers close to the stimulus electrode (Figure 2A-D). The maximal peak PSC amplitude was regarded as the maximal MNTB input the LSO neuron received. On average, the maximal MNTB-evoked responses increased approximately 6-fold from 0.75 ± 0.12 nA in neonates (P1-3, n = 26) to 4.79 ± 0.64 nA in the hearing onset group (P10-12, n = 31) (Figure 2E and F). Taking into account the -50 mV of driving force on chloride under our recording conditions, the maximal synaptic conductance (peak current divided by driving force) increased on average from 15.0 ± 2.4 nS (range: 2-51 nS, P1-3) to 95.8 ± 12.8 nS (range: 7-313 nS, P10-12).

We next recorded PSCs elicited by the activation of single MNTB fibers using minimal stimulation technique (see Methods). As illustrated in **3A-D**, the first responses that emerged from failures were taken as single-fiber PSCs. From P1 to P12, these single-fiber PSC amplitudes increased about 14-fold from 34 ± 7 pA (P1-3, n = 22) to 470 ± 93 pA (P10-12, n = 34) (Figure 3E and F). By dividing the mean maximal amplitude by the mean amplitude of single-fiber PSCs, we estimate that in neonate mice approximately 22 weak MNTB fibers innervate a single LSO neuron, whereas around hearing onset approximately 10 strong MNTB fibers converge onto single LSO neurons. Thus before hearing onset in 129S6/SvEv mice, approximately a half of the initial MNTB inputs that converge on single LSO neurons are functionally eliminated.

Development of quantal size

The increase in the amplitude of MNTB-evoked PSCs can result from an increase in quantal amplitude, release probability, and number of release sites. To determine whether an increase in quantal size contributes to the 14-fold increase in single-fiber PSCs, we recorded miniature PSCs (mPSCs) generated specifically from MNTB axon terminals by electrically stimulating MNTB fibers in an extracellular solution containing 2 mM Sr^{2+} / 0 mM Ca^{2+}. This condition promotes asynchronous release, allowing individual quantal events to be resolved (Goda and Stevens, 1994; Xu-Friedman and Regehr, 1999). Because in the mouse MNTB-LSO, single stimuli only very rarely elicited asynchronous events, we stimulated MNTB axons with a train of electrical stimuli at 100 Hz (2 to 10 shocks) (Figure 4A and B). From P1-3 to P10-12, the mean peak amplitudes of evoked mPSCs increased 2-fold from 30 ± 5 pA (P1-3, n = 6) to 59 ± 9 pA (P10-12, n = 7) (Figure 4 C-F). This 2-fold increase in quantal size contributes to the 14-fold increase in single-fiber PSC. It indicates, however, that a large increase in single-fiber quantal content from 1 (P1-3: 34 pA/30 pA) to 8 (P10-12: 470 pA/59 pA) is the major change underlying the strengthening.

Development of paired-pulse responses of MNTB inputs

We next investigated whether an increase in release probability and thus an increase in the number of vesicles released per action potential contributes to the increase in single-fiber PSCs. Paired pulse ratios (PPRs) are commonly used to probe changes in release probability (Zucker, 1989; Debanne et al., 1996; von Gersdorff and Borst, 2002). Paired-pulse facilitation (PPF; PPR > 1) is generally accepted as an indication of low release probability while paired pulse depression (PPD; PPR < 1) indicates a high release probability. PPRs at varying interstimulus intervals were recorded at stimulus intensities at which PSC amplitudes were maximal (200-400 μA) to minimize fluctuations in the number of fibers activated between two pulses. At stimulus intervals of 10 and 20 ms, responses to the second pulse were significantly more depressed in the younger animals (PPR = 0.66 and 0.82, P1-3, n = 8) than in the older animals (PPR = 0.93 and 0.95, P10-12, n = 9) (Figure 5A and B). At 50 ms and longer intervals, PPRs were higher than 0.9 or in both age groups, and values were not statistical different between age groups (Figure 5A and B). The decrease in PPD with age suggests that MNTB terminals in the LSO of neonatal animals have a higher release probability than in P10-12 animals (Pouzat and Hestrin, 1997; Brenowitz and Trussell, 2001).

Paired pulse depression can be caused not only by a reduction in presynaptic release, but also by postsynaptic mechanisms such as receptor desensitization and saturation (Jones and Westbrook, 1995; Chen et al., 2002). To test for a contribution of postsynaptic mechanisms we analyzed the coefficient of variation (CV = std / mean) for the paired-pulse responses. In a binomial model, if PPD occurs due to a postsynaptic mechanism, $1/CV^2$ of the peak amplitudes is unchanged between the first PSC and the second PSC, while the mean amplitude decreases. This results in data points above the diagonal in $1/CV^2$ ratio vs. mean ratio plot. On the other hand, if PPD is caused by reduced presynaptic release, points will fall below or on the diagonal because $1/CV^2$ will decrease more than the mean (Malinow and Tsien, 1990; Kraushaar and Jonas, 2000; Pedroarena and Schwarz, 2003; Sjostrom et al., 2003). The CV values were computed from individual paired-pulse responses at 10 and 20 ms intervals in P1-3 LSO neurons that showed a clear PPD (PPR < 0.9) (6 cases at 10 ms and 4 cases at 20 ms), and $1/CV^2$ and mean of the second PSCs normalized to those of the first PSCs were plotted (Figure 5C). Most points in this plot fell below the diagonal, indicating a presynaptic origin of the observed PPD. Taken together our results suggest that release probability is higher in younger animals, making it unlikely that an increased release probability is responsible for the developmental increase in MNTB PSC amplitudes.

Potential contribution of developmental relocation of synapse location

Principal neurons of the LSO have a substantial dendritic tree (Helfert and Schwartz, 1987; Kandler and Friauf, 1995a; Rietzel and Friauf, 1998). Because all our recordings were made from the soma, the dendritic location of synaptic inputs could also influence PSC amplitudes due to dendritic filtering (Hausser et al., 2000). In the developing medial superior olive (MSO) of gerbils there is an age-dependent shift of synapse location towards the soma (Kapfer et al. 2002), but it is unknown whether a similar subcellular redistribution of synapses also occurs in the LSO. To examine whether a possible distal to proximal shift of synapse location may account for the apparent increase in MNTB fiber strength we analyzed the rise time of PSCs.

The mean 20-80% rise time of single-fiber PSC was 0.75 ± 0.05 ms in younger animals (P1-3, n = 22) and 0.37 ± 0.02 ms in older animals (P10-12, n = 34) (Figure 6A). This 2-fold reduction in rise time may indicate a distal to proximal shift in synapse location during development. However, the rise time of synaptic responses is also influenced by other factors such as neurotransmitter concentration in the synaptic cleft and postsynaptic receptor distribution (Ali et al., 2000). Therefore, if dendritic filtering indeed is a major contributing factor in determining PSC amplitudes one would expect a negative correlation between rise times and amplitudes as dendritic filtering would both decrease speed and amplitudes. In contrast to this expectation, however, no significant correlation between rise times of single-fiber PSCs and their amplitudes was present at either age group (Figure 6B and C; P1-3: 328 PSCs pooled across cells, r = -0.018, P = 0.75; P10-12: 550 PSCs, r = -0.062, P = 0.14). In younger animals, PSCs with faster rise times (< 0.5 ms, thus comparable to the older group) were as small as those with slower rise times, suggesting proximal inputs had also small amplitudes (Figure 6B). In older animals, most of the small-amplitude inputs (< 100 pA) had rise times similar or identical to those of large-amplitude inputs (> 1000 pA) (Figure 6C). Therefore, in the older age group, differences in PSC amplitudes are not due to different degrees of dendritic filtering. Together, these data suggest that soma-dendritic synapse redistribution is not a major contributor to the 14-fold increase in single-fiber PSCs.

Discussion

In this study, we demonstrate that synapse elimination and strengthening are prominent events in the development of the MNTB-LSO pathway of neonatal 129S6/SvEv mice before hearing onset and that developmental strengthening of unitary MNTB-LSO connections is achieved primarily by a 2-fold increase in quantal size and an 8-fold increase in the quantal content of single-axon MNTB-LSO connections.

Refinement of the mouse MNTB-LSO pathway

Based on single-fiber and maximal responses, we estimate that the number of MNTB inputs converging onto a single LSO neuron decreases from approximately 22 in newborn animals to approximately 10 at hearing onset. During the same developmental period, a substantial, 14-fold strengthening of maintained fibers takes place that outweighs the loss of inputs. In evaluating these numbers one needs to consider that the exact values of these estimations may be influenced by several potential sources of error. First, all of our experiments were conducted in slices in which some MNTB axons likely were severed. Thus, our convergence estimation probably underestimates the actual number of converging inputs present *in vivo*. Second, the analysis of single-fiber responses relies on the premise that recruitment of MNTB fibers by electrical stimuli occurs independently of their strengths. We think that this is likely because we did not observe a correlation between minimal stimulation currents and single-fiber strength. Finally, especially in the older age group, both single-fiber and maximal responses exhibited a wide range of amplitudes, which may introduce uncertainty

in the exact number of converging inputs. For instance, if relatively small maximal responses were due to severing of inputs by slicing, one would expect the convergence estimated from cells with large maximal responses would be higher and represent a better estimation. To test this possibility, we selected 29 cells (P10-12) in which we recorded both single-fiber and maximal responses and divided them into two groups by their maximal responses (i.e., cells with maximal responses below median and above median). Our result showed that the convergence calculated in the cells with smaller maximal responses (below median) was not different from the convergence in the cells with larger maximal responses (above median) (9.4 vs 9.6). This indicates that our convergence estimations are not determined by the size of maximal responses. Thus the variability in the observed convergence ratios likely reflects a biological variability rather then is due to variations in experimental parameters such as the proportion intact MNTB-LSO pathway in the slices. Taken together, while these factors may influence the exact values of our estimates, our results nevertheless indicate a clear and substantial reduction in the convergence ratio before hearing onset. As summarized in Table 1, this conclusion is further supported because the degree of refinement we observed in 129S6/SvEv mice is comparable to the degree of refinement in another strain of mice (Noh et al., 2010) and in prehearing rats (Kim and Kandler, 2003) both in respect to the reduction in convergence ratio (76% in rats vs. 55% reported here) and in respect to the strengthening of individual fibers (12 fold in rats vs.14 fold reported here). In the gerbil LSO, reduction in convergence was also reported, but the reduction occurred gradually both before and after hearing onset (~15 at P1-7 to ~9 at P17-23; Sanes, 1993). Thus, synapse elimination and strengthening in the MNTB-LSO pathway before hearing onset seems to be a general developmental process in rodents, with a possible exception of gerbils, and also perhaps in other mammalian species.

Synaptic mechanisms underlying the strengthening of single MNTB-LSO connections

From P1 to P12, the amplitudes of mPSCs at MNTB-LSO synapses increased by about 2-fold. Both the absolute amplitudes and the percent increase of evoked mPSCs are comparable to GABA/glycinergic mPSC that have been recorded in dissociated rat LSO neurons in TTX over a similar developmental period (mouse, this study, 30 to 59 pA; rat, Nabekura et al., 2004, ~25 to ~55 pA, same driving force for Cl^- current) suggesting that Sr^{2+} does not affect mPSC amplitudes. Although we cannot exclude the possibility of changes in single channel conductance, the developmental increase in quantal amplitude most likely reflects an increase in the number of postsynaptic $GABA_A$ and glycine receptors (Singer and Berger, 1999). More detailed analysis of the quantal events such as nonstationary fluctuation analysis may shed light on this issue (Sigworth, 1980; Traynelis et al., 1993; De Koninck and Mody, 1994). Antibody staining against α1 glycine receptors initially is weak and diffuse in LSO neurons but becomes more intense and clustered during the first two postnatal weeks (Friauf et al., 1997). Albeit not quantitative, these data, together with the increase in the level of α1 mRNA (Piechotta et al., 2001), suggest an increase in glycine receptor expression. In the anteroventral cochlear nucleus larger glycine receptor cluster size correlate with larger mIPSC amplitudes (Lim et al., 1999). In the spinal cord and other brain areas, a developmental switch of glycine receptor subunit has been observed, where initially α2 subunit is predominant, but later replaced by α1 subunit (Betz et al., 1994). At least in the rat LSO, this switch does not seem to occur because the level of mRNA for α2 subunit is very low at birth and remains low, while α1 mRNA level increases during the first two postnatal weeks (Piechotta et al., 2001). It needs to be determined whether other mechanisms, such as an increase in single-channel conductances, channel opening times, or a reduction in dendritic filtering (Otis et al., 1994; Hausser et al., 2000), additionally contribute to the increase in mPSC amplitudes.

The signals that regulate the increase in quantal amplitude at MNTB-LSO synapses are unknown but may involve homeostatic mechanisms triggered by the silencing of MNTB inputs. An increase in glycinergic quanta has been described in cultured mouse spinal neurons after pharmacological blockade of glycine receptors (Carrasco et al., 2007) and in MNTB neurons of congenitally deaf dn/dn mice (Leao et al., 2004). Homeostatic scaling of GABAergic quanta following changes in excitatory activity has also been observed in a variety of neuronal systems (Otis et al., 1994; Kilman et al., 2002; Gonzalez-Forero et al., 2005). However, in the developing LSO of gerbils, a decrease in glutamatergic synaptic activity due to cochlear ablation does not significantly change MNTB-elicited responses (Kotak and Sanes, 1997) suggesting that homeostatic scaling in LSO neurons, if present, is independent of excitatory inputs.

Despite the 2-fold increase in the amplitudes of mPSCs, an increase in quantal size can account for only about 14% of the observed 14-fold increase in single-fiber PSC amplitude. In addition, the decrease in PPD over the same period (Figure 5) argues against the possibility that an increase in neurotransmitter release underlies the strengthening of single MNTB fibers. Therefore, the most likely mechanism responsible for the large increase of single-fiber MNTB-LSO connections is the addition of new release sites formed by individual MNTB axons onto single LSO neurons.

Consistent with this view, the average quantal content of single-fiber PSCs rose from 1 at P1-3 to 8 at P10-12. Although the actual number of release sites is difficult to determine, a mean quantal content of 1 in newborn animals suggests that at this age, an action potential in individual MNTB fibers activates neurotransmitter release from only one or very few functional release sites. Around hearing onset, however, the average MNTB fiber has at least 8 functional release sites and this number likely is considerably higher if one considers a PPR close to 1 at pulse intervals of 10 ms. Such an age-dependent increase in the number of release sites formed by unitary connections also underlies the developmental strengthening of GABAergic connections in the superior colliculus (Juttner et al., 2001), somatosensory, and visual cortex (Morales et al., 2002; Kobayashi et al., 2008).

Developmental changes in the strength of inhibitory connections also occur in other nuclei of the superior olivary complex. In MNTB principal neurons, the strength of single-fiber GABA/glycinergic inputs increases about 10 fold during the second postnatal week (Awatramani et al., 2005). Similar to the LSO, this increase is mediated by a combination of an increase in quantal size (~ 2-fold) and increase in the number of release sites. In the gerbil MSO, in which MNTB inputs are refined after the onset of hearing (Kapfer et al., 2002; Werthat et al., 2008), quantal sizes decrease by about 50% during the first week after hearing onset (P12 – 20) when MNTB axons are pruned. This decrease in quantal size depends on normal acoustic experience (Magnusson et al., 2005). It remains to be shown whether the changes we observed in the LSO during refinement are influenced by spontaneous excitatory or inhibitory activity before hearing onset.

Acknowledgments

We thank Kristi Cihil for technical support. This study was supported by NIDCD (004199)

References

Ali DW, Drapeau P, Legendre P. Development of spontaneous glycinergic currents in the Mauthner neuron of the zebrafish embryo. J Neurophysiol. 2000; 84:1726–1736. [PubMed: 11024065]

Awatramani GB, Turecek R, Trussell LO. Staggered development of GABAergic and glycinergic transmission in the MNTB. J Neurophysiol. 2005; 93:819–828. [PubMed: 15456797]

Behrends JC, ten Bruggencate G. Changes in quantal size distributions upon experimental variations in the probability of release at striatal inhibitory synapses. J Neurophysiol. 1998; 79:2999–3011. [PubMed: 9636103]

Betz H, Kuhse J, Fischer M, Schmieden V, Laube B, Kuryatov A, Langosch D, Meyer G, Bormann J, Rundstrom N. Structure, diversity and synaptic localization of inhibitory glycine receptors. J Physiol Paris. 1994; 88:243–248. Review. [PubMed: 7874085]

Bledsoe SC, Snead CR, Helfert RH, Prasad V, Wenthold RJ, Altschuler RA. Immunocytochemical and lesion studies support the hypothesis that the projection from the medial nucleus of the trapezoid body to the lateral superior olive is glycinergic. Brain Res. 1990; 517:189–194. [PubMed: 2375987]

Boudreau JC, Tsuchitani C. Binaural interaction in the cat superior olive S segment. J Neurophysiol. 1968; 31:442–454. [PubMed: 5687764]

Brenowitz S, Trussell LO. Maturation of synaptic transmission at end-bulb synapses of the cochlear nucleus. J Neurosci. 2001; 21:9487–9498. [PubMed: 11717383]

Cant NB, Casseday JH. Projections from the anteroventral cochlear nucleus to the lateral and medial superior olivary nuclei. J Comp Neurol. 1986; 247:457–476. [PubMed: 3722446]

Carrasco MA, Castro PA, Sepulveda FJ, Cuevas M, Tapia JC, Izaurieta P, van ZB, Aguayo LG. Anti-homeostatic synaptic plasticity of glycine receptor function after chronic strychnine in developing cultured mouse spinal neurons. J Neurochem. 2007; 100:1143–1154. [PubMed: 17217420]

Chen C, Blitz DM, Regehr WG. Contributions of receptor desensitization and saturation to plasticity at the retinogeniculate synapse. Neuron. 2002; 33:779–788. [PubMed: 11879654]

Clements JD, Bekkers JM. Detection of spontaneous synaptic events with an optimally scaled template. Biophys J. 1997; 73:220–229. [PubMed: 9199786]

De Koninck Y, Mody I. Noise analysis of miniature IPSCs in adult rat brain slices: properties and modulation of synaptic GABAA receptor channels. J Neurophysiol. 1994; 71:1318–1335. [PubMed: 8035217]

Debanne D, Gahwiler BH, Thompson SM. Cooperative interactions in the induction of long-term potentiation and depression of synaptic excitation between hippocampal CA3-CA1 cell pairs in vitro. Proc Natl Acad Sci U S A. 1996; 93:11225–11230. [PubMed: 8855337]

Friauf, E. Developmental changes and cellular plasticity in the superior olivary complex. In: Parks, TN.; Rubel, EW.; Fay, RR.; Popper, AN., editors. Plasticity of the Auditory System. New York: Springer; 2004. p. 49-95.

Friauf E, Hammerschmidt B, Kirsch J. Development of adult-type inhibitory glycine receptors in the central auditory system of rats. J Comp Neurol. 1997; 385:117–134. [PubMed: 9268120]

Geal-Dor M, Freeman S, Li G, Sohmer H. Development of hearing in neonatal rats: Air and bone conducted ABR thresholds. Hearing Res. 1993; 69:236–242.

Goda Y, Stevens CF. Two components of transmitter release at a central synapse. Proc Natl Acad Sci U S A. 1994; 91:12942–12946. [PubMed: 7809151]

Gonzalez-Forero D, Pastor AM, Geiman EJ, itez-Temino B, Alvarez FJ. Regulation of gephyrin cluster size and inhibitory synaptic currents on Renshaw cells by motor axon excitatory inputs. J Neurosci. 2005; 25:417–429. [PubMed: 15647485]

Hausser M, Spruston N, Stuart GJ. Diversity and dynamics of dendritic signaling. Science. 2000; 290:739–744. [PubMed: 11052929]

Helfert RH, Schwartz IR. Morphological features of five neuronal classes in the gerbil lateral superior olive. Am J Anat. 1987; 179:55–69. [PubMed: 3618521]

Ishizuka K, Chen J, Taya S, Li W, Millar JK, Xu Y, Clapcote SJ, Hookway C, Morita M, Kamiya A, Tomoda T, Lipska BK, Roder JC, Pletnikov M, Porteous D, Silva AJ, Cannon TD, Kaibuchi K, Brandon NJ, Weinberger DR, Sawa A. Evidence that many of the DISC1 isoforms in C57BL/6J mice are also expressed in 129S6/SvEv mice. Mol Psychiatry. 2007; 12:897–899. [PubMed: 17895924]

Jones MV, Westbrook GL. Desensitized states prolong GABAA channel responses to brief agonist pulses. Neuron. 1995; 15:181–191. [PubMed: 7542462]

Juttner R, Meier J, Grantyn R. Slow IPSC kinetics, low levels of alpha1 subunit expression and paired-pulse depression are distinct properties of neonatal inhibitory GABAergic synaptic connections in the mouse superior colliculus. Eur J Neurosci. 2001; 13:2088–2098. [PubMed: 11422449]

Kandler K, Clause A, Noh J. Tonotopic reorganization of developing auditory brainstem circuits. Nat Neurosci. 2009; 12:711–717. [PubMed: 19471270]

Kandler K, Friauf E. Pre- and postnatal development of efferent connections of the cochlear nucleus in the rat. J Comp Neurol. 1993; 328:161–184. [PubMed: 8423239]

Kandler K, Friauf E. Development of electrical membrane properties and discharge characteristics of superior olivary complex neurons in fetal and postnatal rats. Eur J Neurosci. 1995; 7:1773–1790. [PubMed: 7582130]

Kandler K, Gillespie DC. Developmental refinement of inhibitory sound-localization circuits. Trends Neurosci. 2005; 28:290–296. [PubMed: 15927684]

Kapfer C, Seidl AH, Schweizer H, Grothe B. Experience-dependent refinement of inhibitory inputs to auditory coincidence-detector neurons. Nat Neurosci. 2002; 5:247–253. [PubMed: 11850629]

Kilman V, van Rossum MC, Turrigiano GG. Activity deprivation reduces miniature IPSC amplitude by decreasing the number of postsynaptic GABA(A) receptors clustered at neocortical synapses. J Neurosci. 2002; 22:1328–1337. [PubMed: 11850460]

Kim G, Kandler K. Elimination and strengthening of glycinergic/GABAergic connections during tonotopic map formation. Nat Neurosci. 2003; 6:282–290. [PubMed: 12577063]

Kim J, Alger BE. Random response fluctuations lead to spurious paired-pulse facilitation. J Neurosci. 2001; 21:9608–9618. [PubMed: 11739571]

Kobayashi M, Hamada T, Kogo M, Yanagawa Y, Obata K, Kang Y. Developmental profile of GABAA-mediated synaptic transmission in pyramidal cells of the somatosensory cortex. Eur J Neurosci. 2008; 28:849–861. [PubMed: 18691332]

Koike H, Arguello PA, Kvajo M, Karayiorgou M, Gogos JA. Disc1 is mutated in the 129S6/SvEv strain and modulates working memory in mice. Proc Natl Acad Sci U S A. 2006; 103:3693–3697. [PubMed: 16484369]

Kotak VC, Korada S, Schwartz IR, Sanes DH. A developmental shift from GABAergic to glycinergic transmission in the central auditory system. J Neurosci. 1998; 18:4646–4655. [PubMed: 9614239]

Kotak VC, Sanes DH. Deafferentation weakens excitatory synapses in the developing central auditory system. Eur J Neurosci. 1997; 9:2340–2347. [PubMed: 9464928]

Kraushaar U, Jonas P. Efficacy and stability of quantal GABA release at a hippocampal interneuron-principal neuron synapse. J Neurosci. 2000; 20:5594–5607. [PubMed: 10908596]

Kullmann PH, Kandler K. Glycinergic/GABAergic synapses in the lateral superior olive are excitatory in neonatal C57Bl/6J mice. Brain Res Dev Brain Res. 2001; 131:143–147.

Kullmann PH, Kandler K. Dendritic Ca(2+) responses in neonatal lateral superior olive neurons elicited by glycinergic/GABAergic synapses and action potentials. Neuroscience. 2008

Leao RN, Oleskevich S, Sun H, Bautista M, Fyffe RE, Walmsley B. Differences in glycinergic mIPSCs in the auditory brain stem of normal and congenitally deaf neonatal mice. J Neurophysiol. 2004; 91:1006–1012. [PubMed: 14561690]

Lim R, Alvarez FJ, Walmsley B. Quantal size is correlated with receptor cluster area at glycinergic synapses in the rat brainstem. J Physiol. 1999; 516(Pt 2):505–512. [PubMed: 10087348]

Lu T, Trussell LO. Inhibitory transmission mediated by asynchronous transmitter release. Neuron. 2000; 26:683–694. [PubMed: 10896163]

Magnusson AK, Kapfer C, Grothe B, Koch U. Maturation of glycinergic inhibition in the gerbil medial superior olive after hearing onset. J Physiol. 2005; 568:497–512. [PubMed: 16096336]

Malinow R, Tsien RW. Presynaptic enhancement shown by whole-cell recordings of long-term potentiation in hippocampal slices. Nature. 1990; 346:177–180. [PubMed: 2164158]

Morales B, Choi SY, Kirkwood A. Dark rearing alters the development of GABAergic transmission in visual cortex. J Neurosci. 2002; 22:8084–8090. [PubMed: 12223562]

Nabekura J, Katsurabayashi S, Kakazu Y, Shibata S, Matsubara A, Jinno S, Mizoguchi Y, Sasaki A, Ishibashi H. Developmental switch from GABA to glycine release in single central synaptic terminals. Nat Neurosci. 2004; 7:17–23. [PubMed: 14699415]

Noh J, Seal RP, Garver JA, Edwards RH, Kandler K. Glutamate co-release at GABA/glycinergic synapses is crucial for the refinement of an inhibitory map. Nat Neurosci. 2010; 13:232–238. [PubMed: 20081852]

Otis TS, De Koninck Y, Mody I. Lasting potentiation of inhibition is associated with an increased number of gamma-aminobutyric acid type A receptors activated during miniature inhibitory postsynaptic currents. Proc Natl Acad Sci U S A. 1994; 91:7698–7702. [PubMed: 8052645]

Pedroarena CM, Schwarz C. Efficacy and short-term plasticity at GABAergic synapses between Purkinje and cerebellar nuclei neurons. J Neurophysiol. 2003; 89:704–715. [PubMed: 12574448]

Piechotta K, Weth F, Harvey RJ, Friauf E. Localization of rat glycine receptor alpha1 and alpha2 subunit transcripts in the developing auditory brainstem. J Comp Neurol. 2001; 438:336–352. [PubMed: 11550176]

Pouzat C, Hestrin S. Developmental regulation of basket/stellate cell-->Purkinje cell synapses in the cerebellum. J Neurosci. 1997; 17:9104–9112. [PubMed: 9364057]

Rietzel HJ, Friauf E. Neuron types in the rat lateral superior olive and developmental changes in the complexity of their dendritic arbors. J Comp Neurol. 1998; 390:20–40. [PubMed: 9456173]

Sanes DH. The development of synaptic function and integration in the central auditory system. J Neurosci. 1993; 13:2627–2637. [PubMed: 8501528]

Sanes DH, Friauf E. Development and influence of inhibition in the lateral superior olivary nucleus. Hear Res. 2000; 147:46–58. [PubMed: 10962172]

Sanes DH, Rubel EW. The ontogeny of inhibition and excitation in the gerbil lateral superior olive. J Neurosci. 1988; 8:682–700. [PubMed: 3339433]

Sanes DH, Siverls V. Development and specificity of inhibitory terminal arborizations in the central nervous system. J Neurobiol. 1991; 8:837–854. [PubMed: 1663990]

Schurov IL, Handford EJ, Brandon NJ, Whiting PJ. Expression of disrupted in schizophrenia 1 (DISC1) protein in the adult and developing mouse brain indicates its role in neurodevelopment. Mol Psychiatry. 2004; 9:1100–1110. [PubMed: 15381924]

Sigworth FJ. The variance of sodium current fluctuations at the node of Ranvier. J Physiol. 1980; 307:97–129. [PubMed: 6259340]

Singer JH, Berger AJ. Contribution of single-channel properties to the time course and amplitude variance of quantal glycine currents recorded in rat motoneurons. J Neurophysiol. 1999; 81:1608–1616. [PubMed: 10200197]

Sjostrom PJ, Turrigiano GG, Nelson SB. Neocortical LTD via coincident activation of presynaptic NMDA and cannabinoid receptors. Neuron. 2003; 39:641–654. [PubMed: 12925278]

Sommer I, Lingenhöhl K, Friauf E. Principal cells of the rat medial nucleus of the trapezoid body: An intracellular in vivo study of their physiology and morphology. Exp Brain Res. 1993; 95:223–239. [PubMed: 8224048]

Stevens CF, Wang Y. Changes in reliability of synaptic function as a mechanism for plasticity. Nature. 1994; 371:704–707. [PubMed: 7935816]

Tollin DJ. The lateral superior olive: a functional role in sound source localization. Neuroscientist. 2003; 9:127–143. [PubMed: 12708617]

Traynelis SF, Silver RA, Cull-Candy SG. Estimated conductance of glutamate receptor channels activated during EPSCs at the cerebellar mossy fiber-granule cell synapse. Neuron. 1993; 11:279–289. [PubMed: 7688973]

von Gersdorff H, Borst JG. Short-term plasticity at the calyx of held. Nat Rev Neurosci. 2002; 3:53–64. [PubMed: 11823805]

Werthat F, Alexandrova O, Grothe B, Koch U. Experience-dependent refinement of the inhibitory axons projecting to the medial superior olive. Dev Neurobiol. 2008; 68:1454–1462. [PubMed: 18777566]

Xu-Friedman MA, Regehr WG. Presynaptic strontium dynamics and synaptic transmission. Biophys J. 1999; 76:2029–2042. [PubMed: 10096899]

Zucker RS. Short-term synaptic plasticity. Annu Rev Neurosci. 1989; 12:13–31. [PubMed: 2648947]

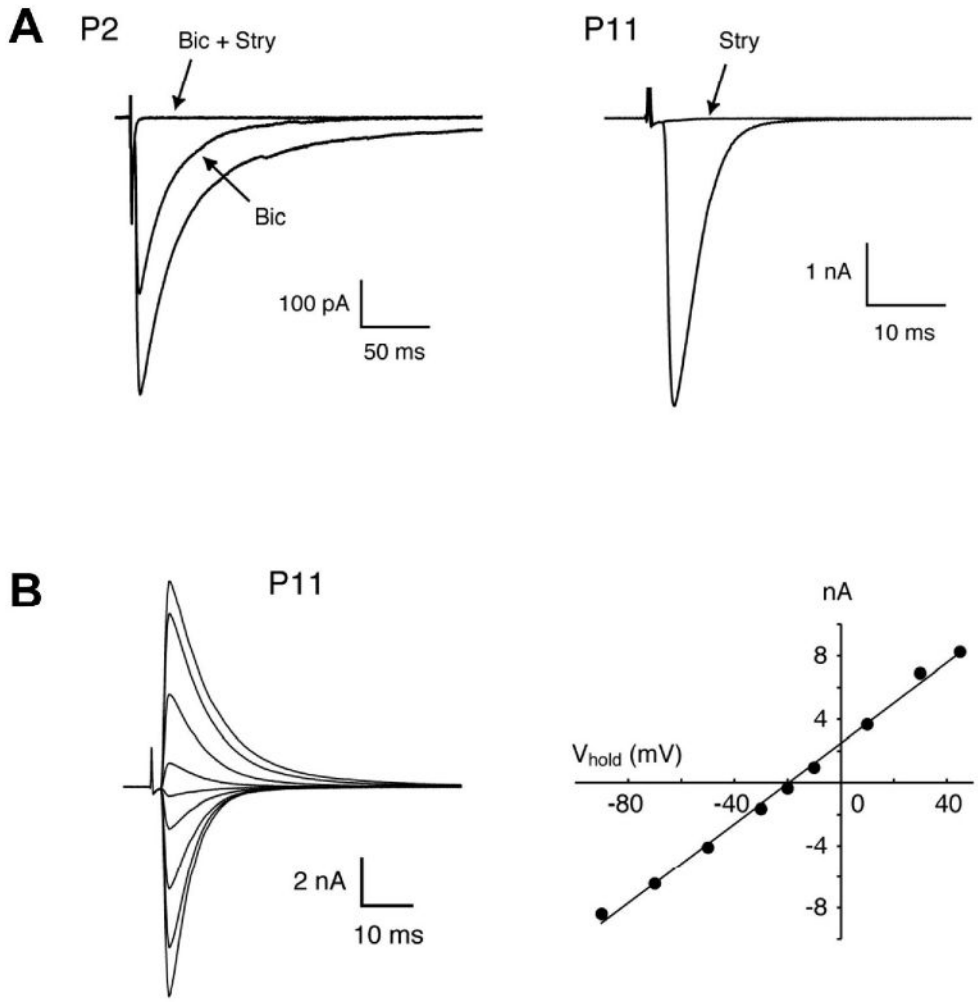

Fig. 1.

MNTB-evoked responses in the developing mouse LSO. (A) Examples of two MNTB-evoked PSCs recorded from a P2 and a P11 LSO neuron. In the P2 animal, peak amplitude was reduced by 37% by 10 μM bicuculline (Bic) and the remaining current was blocked by 1 μM strychnine (Stry). In the P11 animal, the response was completely blocked by 1 μM strychnine. (B) Reversal potential of large MNTB-evoked responses in a P11 LSO neuron. The current-voltage relationship was linear (r = 0.998) and the reversal potential was -19.5 mV, close to the calculated value of -20 mV.

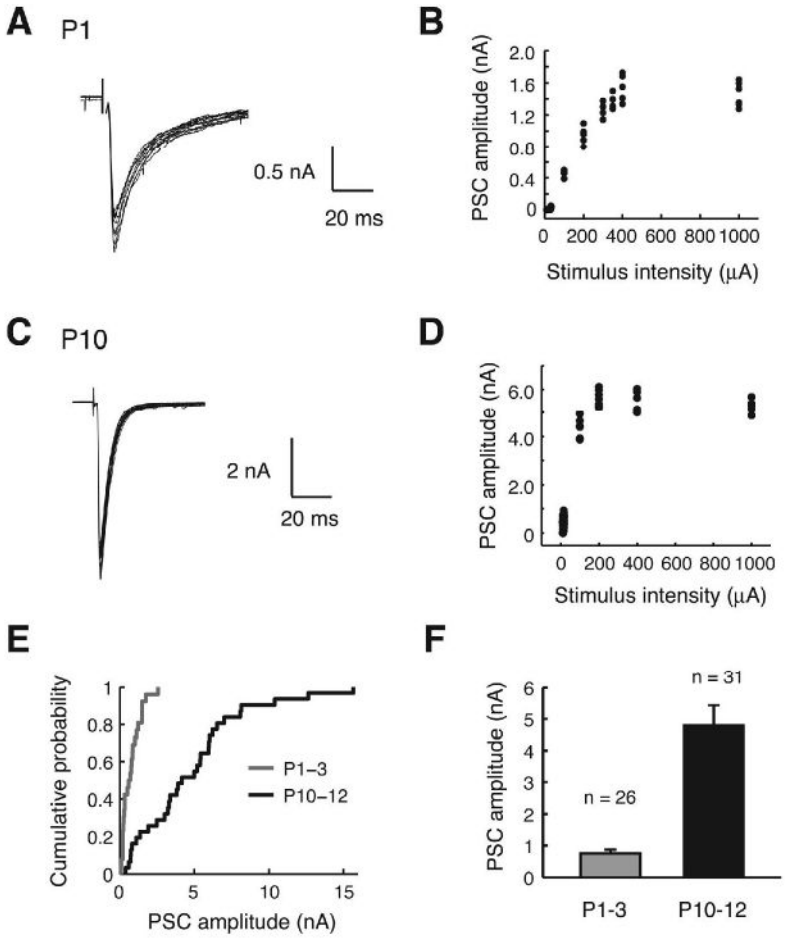

Fig. 2.

Maximal MNTB-evoked responses. (A) Example of maximal PSCs elicited by MNTB stimulation in a P1 LSO neuron (overlay of 10 traces) and (B) the corresponding stimulus-response relationship. (C-D) Example of maximal PSCs in a P10 neuron (overlay of 19 traces) and the corresponding stimulus-response relationship. (E) Cumulative probability distribution of maximal PSC amplitudes. (F) Mean maximal PSC amplitudes in both age groups ($P < 0.01$, Student's t test).

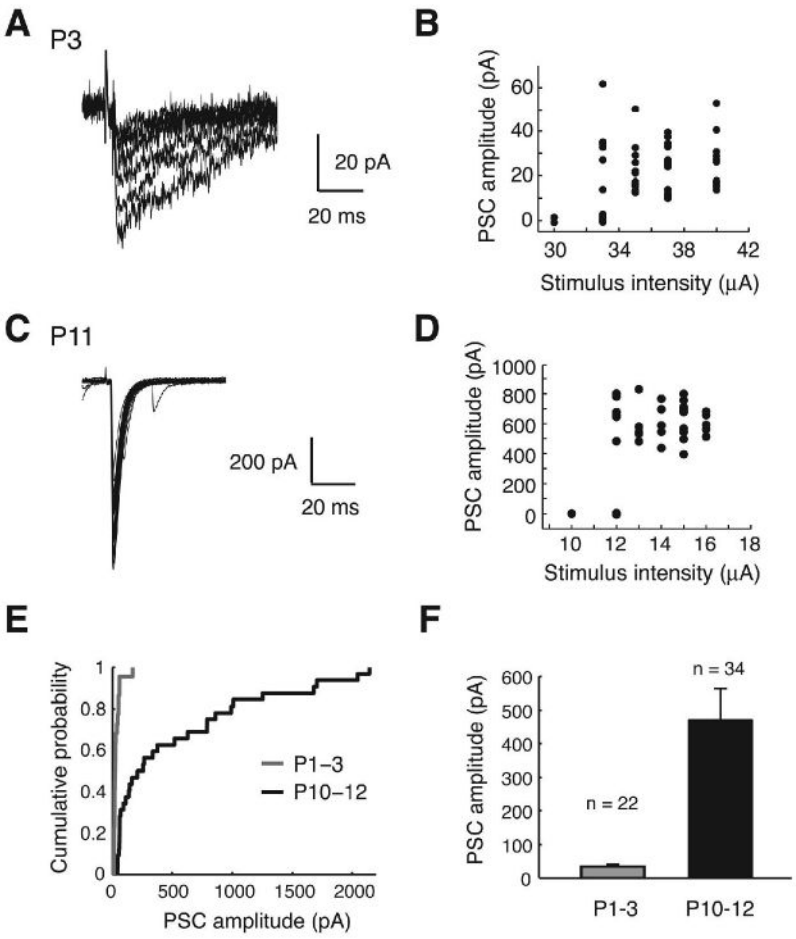

Fig. 3.

Minimal stimulation responses in LSO (A-D) Example traces and stimulus-response relationships of single-fiber PSCs at P2 (overlay of 7 traces) and P10 (overlay of 7 traces). (E) Cumulative probability distribution of single-fiber PSC amplitudes. (F) Mean single-fiber PSC amplitudes ($P < 0.01$, Student's t test).

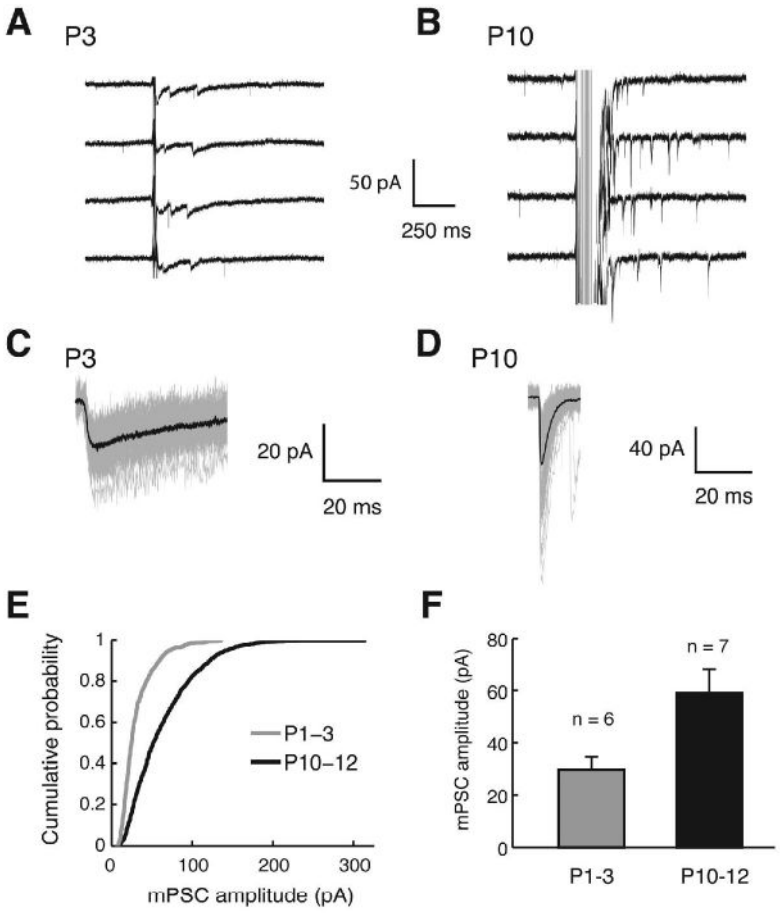

Fig. 4.

Evoked mPSCs elicited by MNTB stimulation in Sr^{2+}. (A-B) Example traces from a P3 and P10 LSO neuron. At P3 a train of stimuli at 100 Hz with two pulses was used, and at P10, 10 pulses at 100 Hz were used to induce asynchronous events. (C-D) Examples of evoked mPSCs aligned at the maximal rise. Black traces are the averages of 50 (P3) and 70 (P10) events, grey traces are individual events. (E) Cumulative histogram of evoked mPSCs pooled across the cells. A total of 823 (P1-3) and 1348 (P10-12) events from 6 and 7 cells, respectively, were plotted ($P < 0.01$, Kolmogorov-Smirnov test). (F) Mean amplitudes of evoked mPSCs ($P < 0.01$, Wilcoxon ranksum test).

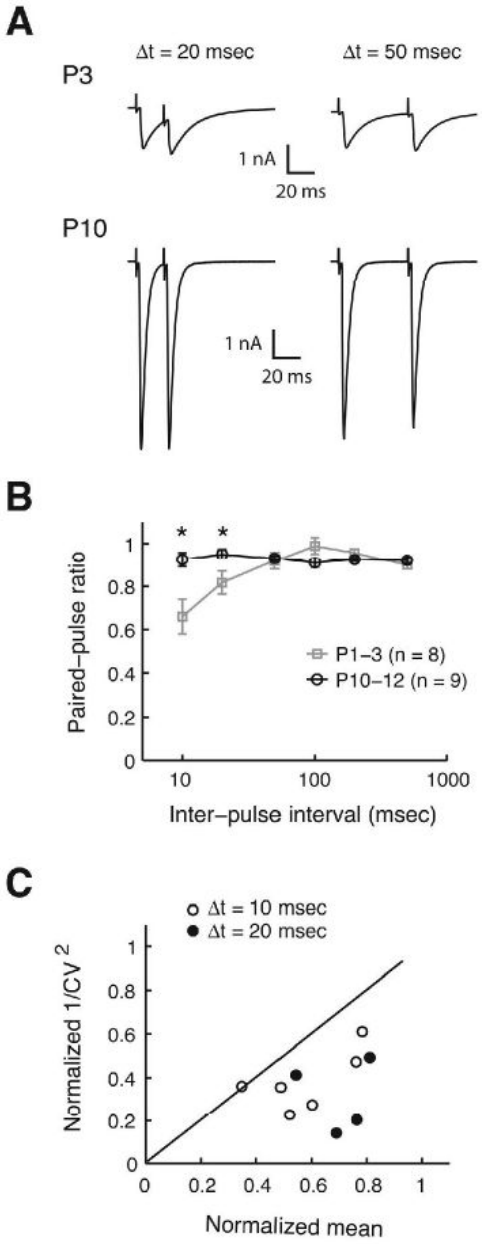

Fig. 5.

Paired-pulse responses of MNTB-evoked responses. (A) Example traces of paired-pulse responses from a P3 and P10 LSO neurons at 20 and 50 ms inter-pulse intervals. (B) Summary of paired pulse ratios at inter-pulse intervals of 10, 20, 50, 100, 200, and 500 ms shown in semi-logarithmic scale (asterisks indicate $P < 0.05$, Student's t-test). (C) Analysis of coefficient of variation (CV) of paired pulse responses at 10 and 20 ms intervals. $1/CV^2$ for the second PSCs normalized to $1/CV^2$ for the fist PSC is plotted against the mean amplitude of the second PSCs normalized to that of the first PSCs (open circles: 6 cases at 10 ms interval; filled circles: 4 cases at 20 ms interval; P1-3).

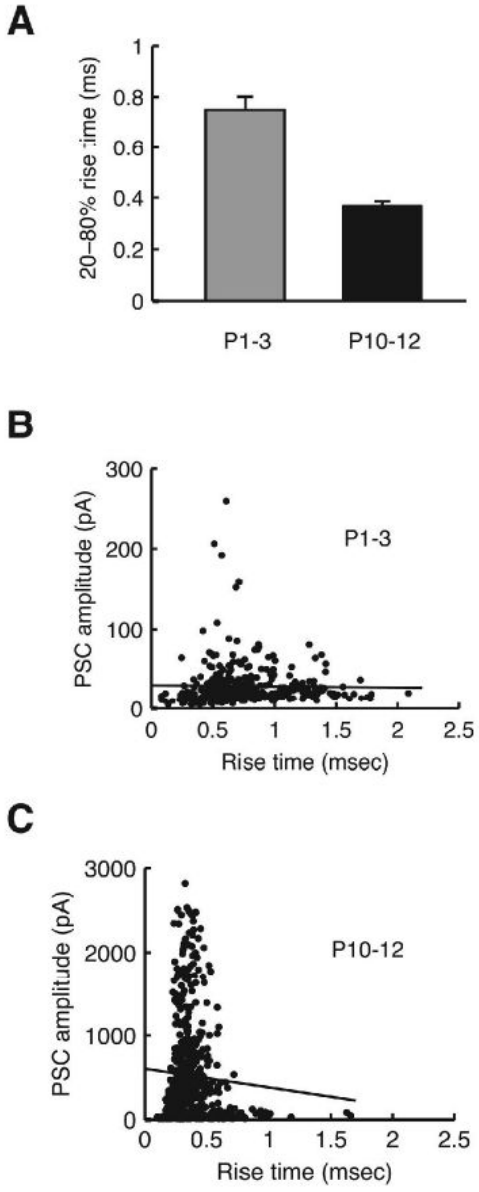

Fig. 6.

Rise times (20-80%) of single-fiber PSCs. (A) Mean rise times of single-fiber PSCs from P1-3 (grey) and P10-12 animals (black). (B) Plot of peak amplitudes vs. rise times for P1-3 animals with a regression line. (C) Plot of peak amplitudes vs. rise times for P10-12 animals with a regression line.

Table 1

Comparison of synaptic transmission among different strains of rats and mice. The data for Sprague-Dawley is from Kim and Kandler (2003) and Nabekura et al. (2004), the data for mouse strain 129S6/SvEv is from the present paper, and the data for the C57Bl/6 mouse strain is from Noh et al.(2010).

	Age	Single-fiber PSC amplitude (pA)	Maximal PSC amplitude (pA)	Estimated convergence	mPSC amplitude (pA)	PPR	
						Δt = 10 msec	Δt = 150-200 msec
Sprague-Dawley	P1-5	57 ± 10	1.4 ± 0.33	25	~25 *	unknown	unknown
	P9-14	719 ± 134	4.5 ± 0.54	6	~55 *	unknown	unknown
129S6/SvEv	P1-3	34 ± 7	0.75 ± 0.12	22	30 ± 5	0.66	0.96
	P10-12	470 ± 93	4.79 ± 0.64	10	59 ± 9	0.93	0.93
Vglut3+/+ (C57Bl/6)	P1-2	71 ± 9	1.3 ± 0.2	19	unknown	unknown	0.9
	P9-12	587 ± 130	4.3 ± 0.5	7	48 ± 3	unknown	0.9

* Theses values are approximate estimates based on Nabekura et al. (2004).